Theory and Applications of Mathematics & Computer Science

(ISSN 2067-2764, EISSN 2247-6202)
http://www.uav.ro/applications/se/journal/index.php/tamcs

Theory and Applications of Mathematics & Computer Science 8 (1) (2018) 39 – 59

Maximal Centroidal Vortices in Triangulations. A Descriptive Proximity Framework in Analyzing Object Shapes

M.Z. Ahmad[a], James Peters[a,b,*]

[a]*Computational Intelligence Laboratory, Department of Electrical & Computer Engineering, University of Manitoba, Winnipeg, MB, R3T 5V6, Canada.*
[b]*Department of Mathematics, Faculty of Arts and Sciences, Adıyaman University, Adıyaman, Turkey.*

Abstract

This paper introduces a framework for approximating visual scene object shapes captured in sequences of video frames. To do this, we consider the hyper-connectedness of image object shapes by extending the Smirnov proximity measure to more than two sets. In this context, a *shape* is a finite, bounded planar region with a nonempty interior. The framework for this work is encapsulated in descriptive frame recurrence diagrams, introduced here. These diagrams offer a new approach in tracking the appearance and eventual disappearance of shapes in studying the persistence of object shapes in visual scenes. This framework is ideally suited for a machine intelligence approach to tracking the lifespans of visual scene structures captured in sequences of images in videos. A practical application of this framework is given in terms of the analysis of vehicular traffic patterns.

Keywords: Hyper-connectedness, Object shape, Proximity, Recurrence, Vortices
2010 MSC No: Primary 54E05 (Proximity), Secondary 68U05 (Computational Geometry).

1. Introduction

A grasp of the persistence and wearout patterns of object shapes in visual scenes is important from a machine intelligence perspective, especially in terms of the increasing need for analytic methods to cope with the high volume of object shape data obtained by video capture devices that monitor our environment. This paper introduces a framework for approximating visual scene surface shapes captured in single digital images and in sequences of video frames. To do this,

*Corresponding author: 75A Chancellor's Circle, EITC-E2-390, University of Manitoba, WPG, MB R3T 5V6, Canada; e-mail: james.peters3@ad.umanitoba.ca, research supported by the Natural Sciences & Engineering Research Council of Canada (NSERC) discovery grant 185986 and Instituto Nazionale di Alta Matematica (INdAM) Francesco Severi, Gruppo Nazionale per le Strutture Algebriche, Geometriche e Loro Applicazioni grant 9 920160 000362, n.prot U 2016/000036.

Email addresses: ahmadmz@myumanitoba.ca (M.Z. Ahmad), James.Peters3@umanitoba.ca (James Peters)

we consider the hyper-connectedness of image objects by extending the Smirnov proximity measure (Smirnov, 1964, §1, pp. 8-10) to more than two sets. It is the topology of cellular complexes introduced by P. Alexandroff (Alexandroff, 1965; Alexandroff & Hopf, 1935; Alexandroff, 1928, 1926), (extended and elaborated by G.E. Cooke and R.L. Finney (Cooke & Finney, 1967)), K. Borsuk (Borsuk, 1948, 1975; Borsuk & Dydak, 1980), a recent formulation of this topology by H. Edelsbrunner and J.L. Harer (Edelsbrunner & Harer, 2010) and the work on persistence homology by E. Munch (Munch, 2013) that provide a solid basis for this study of the object shapes and structures in visual scenes.

2. Preliminaries

A nonempty set K, such that each element in K is contained in a disjoint open set is termed a *Hausdorff space*. Every subset in the partion of K is a *cell*. The *boundary* of a cell A is denoted by $bdy\, A$, and its *closure* by $cl\, A$. The *interior* of a cell is defined as $int\, A = cl\, A - bdy\, A$. A *complex* σ is a collection of subsets in K. σ^n denotes a complex with n cells in K. The closure of a complex is its image under a continuous homomorphic map $f : \sigma^n \to \mathrm{cl}\, \sigma^n$. An *n-skeleton* K^n is the union of all $\sigma^j \in K$ such that $j \leq n$. A CW space is Hausdorff and satisfies the following two conditions:

1^o The closure of each cell $cl\, A\ s.t.\ A \in K$, intersects only a finite number of other cells (**Finite Closure**).

2^o A cell $A \in K$ is closed, provided $A \cap cl\, \sigma^n \neq \emptyset$ is also closed (**Weak Topology**).

Next, consider the structures inherent in a triangulated digital image. In a triangulation of a finite, bounded, planar region K, a collection of triangles A with a common vertex is called a *nerve* (denoted by Nrv$A$). The nerve with the highest number of triangles is called a *maximal nuclear cluster*(MNC). The intersection of an MNC is called the *nucleus*. Each of the triangles in an MNC is called a *1-spoke* (denoted by sk_1). The notion of a 1-spoke can be extended to a *k-spoke*,sk_k, using a recursive definition. All the sets that are not a sk_{k-1}, but have a nonempty intersection with a sk_{k-1} are a sk_k. The nucleus is a 0-spoke (denoted by sk_0). The union of all the $sk_k \in K$ forms a *k-spoke complex* denoted by $skcx_k$.

Nerve spokes lead to two new structures that are useful. A *maximal k-cycle* is a simple closed path connecting the centroids of all the $sk_k \in K$. A closed path has the same start and end points. A simple path has no self-intersections. As a triangualtion can have multiple MNCs, each one has its own maximal k-cycles. Let $mcyc_k(d)$ denote a maximal k-cycle associated with the MNC $d \in K$. A *maximal k-vortex* is the union of all the maximal j-cycles for an MNC $d \in K$,$mcyc_j(d)$, such that $j \leq k$. Let $mvort_k(d)$ be the maximal k-vortex for the MNC $d \in K$.

In a CW topology on a triangulated finite bounded region, two topological spaces are homotopic, provided they can be transformed into one another by means of continuous functions (no tearing and gluing incolved). A classical example is the transformation of a coffee cup to a doughnut and vice versa. An important result linking *nerves* with *homotopy* is the Edelsbrunner-Harer nerve theorem.

Theorem 1. *(Edelsbrunner & Harer, 2010, p. 59). A finite collection of closed, convex sets in Euclidean space, then nerve of the collection is homotopy equivalent to the union of sets in the nerve*

The notion of proximity can be extended from a relation on two as defined previously (Naimpally & Warrack, 1970)(Peters, 2013), to a binary valued function on $n > 2$ sets. This extended notion is termed **hyper-connectedness**. Suppose $A, B \in X$, then $A\delta B$, $A \overset{\curlywedge\curlywedge}{\delta} B$, $A\delta_\Phi B$ represent that A, B are spatial Lodato(δ), strongly($\overset{\curlywedge\curlywedge}{\delta}$) and as descriptively near ($A\delta_\Phi B$), respectively. Similarly, $A \not\delta B$, $A \overset{\curlywedge\curlywedge}{\not\delta} B$, $A\not\delta_\Phi B$ represent that the sets are spatial Lodato, strongly and descriptivly far respectivley. Proximity can also be quantified using the Smirnov proximity measure, defined as $\delta(A, B) = 0$, if the sets A and B are close and $\delta(A, B) = 1$ if the sets A and B are far from each other.

Recall the notation for hyper-connectedness in (Ahmad & Peters, 2017), by extending the Smirnov proximity measure to more than two sets. Suppose $X_1, \cdots, X_n \in X$, then $\delta^n(X_1, \cdots, X_n) = 0$ if they are near and $\delta^n(X_1, \cdots, X_n) = 1$ if they are far. The corresponding hyper-connectedness notions for the proximity relations discussed above are spatial Lodato δ^n, strong $\overset{\curlywedge\curlywedge}{\delta^n}$, and descripticve δ^n_Φ hyper-connectedness. The superscript n represents the number of sets regarding which the notion of proximity is being formulated. For the strong hyper-connectedness $\overset{\curlywedge\curlywedge}{\delta^k}$, the super-script $\curlywedge\curlywedge$ signifies intersection of the interiors required to satisfy this particular relation.

Let $\{A\}_i, B, C \in X$, where $i \in \mathbb{Z}$ is an index set. We define the hyper-connectedness as a function on set X. Moreover, if F is a set then $S(F)$ is the set of all the n-permutations of the elements in F, where $n = |F|$. As an example suppose $F = \{a, b, c\}$, then $S(F) = \{\{a, b, c\}, \{a, c, b\}, \{b, a, c\}, \{b, c, a\}, \{c, a, b\}, \{c, b, a\}\}$. Different types of hyper-connectedness require conformity to varying axioms. The spatial Lodato hyper-connectedness(δ^k) on k sets, requires the following axioms:

(**hP1**) $\forall A_k \subset X, \delta^k(A_1, \cdots, A_k) = 1$, *if any* $A_1, \cdots, A_k = \emptyset$.

(**hP2**) $\delta^k(A_1, \cdots, A_k) = 0 \Leftrightarrow \delta^k(Y) = 0,\ \forall Y \in S(\{A_1, \cdots, A_k\})$.

(**hP3**) $\bigcap_{i=1}^{k} A_i \neq \emptyset \Rightarrow \delta^k(A_1, \cdots, A_k) = 0$.

(**hP4**) $\delta^k(A_1, \cdots, A_{k-1}, B \cup C) = 0 \Leftrightarrow \delta^k(A_1, \cdots, A_{k-1}, B) = 0$ *or* $\delta^k(A_1, \cdots, A_{k-1}, C) = 0$.

(**hP5**) $\delta^k(A_1, \cdots, A_{k-1}, B) = 0$ *and* $\forall b \in B,\ \delta^2(\{b\}, C) = 0 \Rightarrow \delta^k(A_1, \cdots, A_{n-1}, C) = 0$.

(**hP6**) $\forall A \subset X,\ \delta^1(A) = 0$, a constant map.

Next, the definition of strong hyper-connectedness($\overset{\curlywedge\curlywedge}{\delta^k}$) on k sets, requires the following axioms:

(**snhN1**) $\forall A_k \subset X, \overset{\curlywedge\curlywedge}{\not\delta^k}(A_i, \cdots, A_k) = 1$ *if any* $A_1, \cdots, A_k = \emptyset$ *and* $\overset{\curlywedge\curlywedge}{\delta^k}(X, A_1, \cdots, A_{k-1}) = 0, \forall A_i \subset X$.

(**snhN2**) $\overset{\curlywedge\curlywedge}{\delta^k}(A_1, \cdots, A_k) = 0 \Leftrightarrow \overset{\curlywedge\curlywedge}{\delta^k}(Y) = 0,\ \forall Y \in S(\{A_1, \cdots, A_k\})$.

(**snhN3**) $\overset{\curlywedge\curlywedge}{\delta}{}^k(A_1, \cdots, A_k) = 0 \Rightarrow \bigcap_{i=1}^{k} A_i \neq \emptyset$.

(**snhN4**) If $\{B_i\}_{i\in I}$ is an arbitrary family of subsets of X and $\overset{\curlywedge\curlywedge}{\delta}{}^k(A_1, \cdots, A_{k-1}, B_{i^*}) = 0$ for some $i^* \in I$ such that $int(B_{i*}) \neq \emptyset$, then $\overset{\curlywedge\curlywedge}{\delta}{}^n(A_1, \cdots, A_{k-1}, (\bigcup_{i\in I} B_i)) = 0$.

(**snhN5**) $\bigcap_{i=1}^{k} intA_i \neq \emptyset \Rightarrow \overset{\curlywedge\curlywedge}{\delta}{}^k(A_1, \cdots, A_k) = 0$.

(**snhN6**) $x \in \bigcap_{i=1}^{k-1} int(A_i) \Rightarrow \overset{\curlywedge\curlywedge}{\delta}{}^k(x, A_1, \cdots, A_{k-1}) = 0$.

(**snhN7**) $\overset{\curlywedge\curlywedge}{\delta}{}^k(\{x_1\}, \cdots, \{x_k\}) = 0 \Leftrightarrow x_1 = x_2 = \cdots = x_n$.

(**snhN8**) $\forall A \in X, \overset{\curlywedge\curlywedge}{\delta}{}^1(A) = 0$ is a constant map.

Let us define the notion of a descriptive intersection, $A \underset{\Phi}{\cap} B = \{x \in A \cup B : \phi(x) \in \phi(A)\, and\, \phi(x) \in \phi(B)\}$. Here $\phi : K \to \mathbb{R}^n$ is a probe function whic can be seen as a feature extractor. Using these notions, the descriptive hyper-connectedness(δ^k_Φ) on k sets, has the underlying axioms:

(**dhP1**) $\forall A_i \subset X$, $\delta^k_\Phi(A_1, \cdots, A_k) = 1$ if any of the $A_1, \cdots, A_k = \emptyset$.

(**dhP2**) $\delta^k_\Phi(A_1, \cdots, A_k) = 0 \Leftrightarrow \delta^k_\Phi(Y) = 0\, \forall Y \in S(\{A_1, \cdots, A_k\})$.

(**dhP3**) $\underset{\Phi}{\bigcap} A_i \neq \emptyset \Rightarrow \delta^k_\Phi(A_1, \cdots, A_k) = 0$.

(**dhP4**) $\delta^k_\Phi(A_1, \cdots, A_{k-1}, B) = 0\, and\, \forall b \in B$, $\delta^2_\Phi(\{b\}, C) = 0 \Rightarrow \delta^k_\Phi(A_1, \cdots, A_{k-1}, C) = 0$.

(**dhP5**) $\forall A \subset X, \delta^1_\Phi(A) = 0$ a constant map.

The distinctions between different notions of hyper-connectedness are important. The spatial Lodato(δ^k) version allows k sets to be near, provided the sets overlap or asymptotically approach each other. Strong hyper-connectedness($\overset{\curlywedge\curlywedge}{\delta}{}^k$) requires that the sets have non-empty intersection. The descriptive(δ^k_Φ) version allows for the sets to be near, provided the sets contain elements with matching descriptions under the probe functionϕ, regardless of their spatial proximity.

Example 1. *We begin with the notion of Lodato hyper-connectedness(δ^k). The most important thing to note here is that although sharing points implies δ^k, it is not necessary. In addition, asymptotic equality can also qualify sets for Lodato hyper-connectedness. Consider, for example, Fig. 1.1, where A, B, C, D are sets defined by $e^{-0.8x}$, $\frac{\sin x}{4x}$, 0.5, and 0. It must be noted that A approaches D asypmtotically, but B and D intersect at many points. Moreover, B does not share any elements with C, but, A and C intersect. Thus, we can write $\delta^2(A, C) = 0$, $\delta^3(A, B, C) = 0$ and $\delta^4(A, B, C, D) = 1$.*

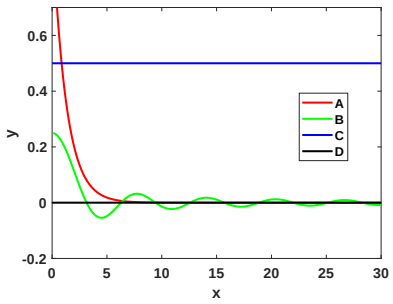

1.1: Lodato hyperconnectedness

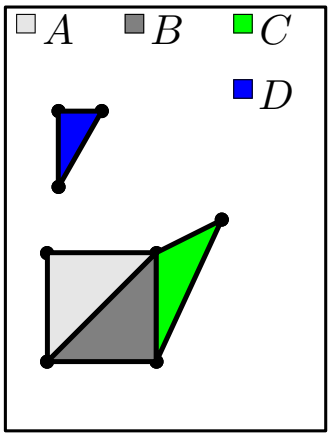

1.2: Strong hyperconnectedness

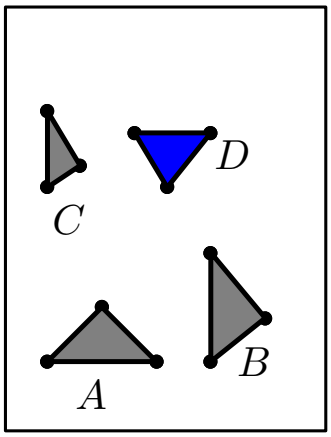

1.3: Descriptive hyperconnectedness

Figure 1: This figure illustrates the different variants of hyperconnectedness. Fig. 1.1 depicts Lodato hyperconnectedness δ^k. Fig.1.2 illustrates the strong hyperconnectedness $\overset{\wedge\wedge}{\delta^k}$ Fig. 1.3 shows descriptive hyperconnectedness δ^k_Φ.

The sets in Fig. 1.2 illustrate the notion of strong hyper-connectedness($\overset{\wedge\wedge}{\delta^k}$). *Observe that* A, B, C *share a common vertex while* D *is disjoint from the remaining sets. We can hence conclude that* $\overset{\wedge\wedge}{\delta^3}(A, B, C) = 0$ *and* $\overset{\wedge\wedge}{\delta^4}(A, B, C, D) = 1$. *The sets in Fig. 1.3 illustrate descriptive hyper-connectedness. We can see that the filled triangles in Fig. 1.3 are spatially disjoint. Triangles* A, B, C *are coloured gray, while* D *is blue. This means that* $\delta^3_\Phi(A, B, C) = 0$ *and* $\delta^4(A, B, C, D) = 1$. ■

Next, consider hyper-connectedness relationships in terms of spoke complexes and maximal centroidal cycles.

Example 2. *Let us first illustrate the idea of spoke complexes(*$skcx_k$*) and the associated maximal centroidal cycles(*$mcyc_k$*), using Fig. 2.1. The notion of maximal nuclear cluster(MNC) is identical to the concept of* $skcx_1$ *as defined in this section. The common intersection of the triangles in* $skcx_1$ *is the nucleus. It is shown as the four triangles shaded gray. The* $skcx_2$ *are represented as green, and have a non-empty intersection with the* $skcx_1$ *but not with the nucleus. Similarly, the* $skcx_3$ *are the red triangles that have a non-empty intersection with* $skcx_2$ *and an empty interesection with* $skcx_1$. *It can be seen that the closed simple path constructed by connecting the centroids of the triangles in a spoke complex is the corresponding maximal centroidal cycle. We can see that* $mcyc_1$ *is shown in red,* $mcyc_2$ *in black and* $mcyc_3$ *is in blue.*

Next, consider proximity and hyper-connectedness of maximal centroidal cycles associated with multiple MNCs in a triangulation. For this consider the illustration in Fig. 2.2. In this figure we have threee different MNCs with three disjoint $skcx_1$ *represented by gray triangles. The red triangles(with slanted lines) are the* $skcx_2$, *but in this case the three MNCs share a triangle which is represented as a red triangle with a crosshatch pattern. We only consider the* $mcyc_2$ *for each of the three different MNCs* A, B, C, *represented as cycA,cycB and cycC.*

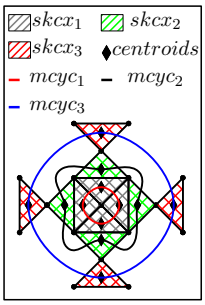

2.1: Maximal Centroidal Cycles

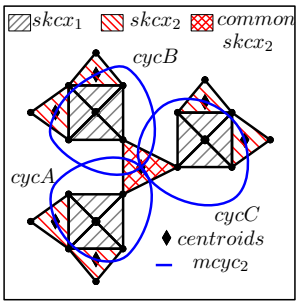

2.2: Hyper-connectedness of *mcyc*

Figure 2: This figure illustrates the concept of maximal centroidal vortex. Fig. 2.1 displays the different maximal centroidal k-cycles, $mcyc_k$ in relation to the corresponding spoke complexes, $skcx_k$. Fig. 2.2 illustrates the notion of hyper-connectedness of *mcyc* for different MNCs.

From the proximity relations we have introduced, we can make a number observations. Observe that $skcx_2A$, δ $skcx_2B$, $skcx_2A\,\delta\,skcx_2C$, $skcx_2B\,\delta\,skcx_2C$ *and* $\delta^3(skcx_2A, skcx_2B, skcx_2C)$. *Similarly, we can say* $mcyc_2A\,\delta\,mcyc_2B$, $mcyc_2A\,\delta\,mcyc_2C$, $mcyc_2B\,\delta\,mcyc_2C$ *and* $\delta^3(mcyc_2A, mcyc_2B, mcyc_2C)$. *As we have seen that the spoke complexes and the cycles share a triangle and centroid respectively, it can be concluded that they share the same description. This leads to* $skcx_2A\,\delta_\Phi\,skcx_2B$, $skcx_2A\,\delta_\Phi\,skcx_2C$, $skcx_2B\,\delta_\Phi\,skcx_2C$, $\delta^3_\Phi(skcx_2A, skcx_2B, skcx_2C)$, $mcyc_2A\,\delta_\Phi\,mcyc_2B$, $mcyc_2A\,\delta_\Phi\,mcyc_2C$, $mcyc_2B\delta_\Phi\,mcyc_2C$ *and* $\delta^3_\Phi(mcyc_2A, mcyc_2B, mcyc_2C)$. ■

3. Main Theoretical Results

Proximity and topology are two ways of talking about how a space is constructed from its subspaces. In this section, we introduce some proximity-related results regarding spoke complexes. Consider first a result for spatial Lodato hyper-connectedness(δ^n) on spoke complexes.

Theorem 2. *Let K a cell complex equipped with a Lodato hyper-connectedness relation. Let $skcx_{k-1}, skcx_k, skcx_{k+1} \in K$ be spoke complexes in K. Then*
1^o $skcx_k \cap skcx_{k+1} \neq \emptyset \Rightarrow \delta^2(skcx_k, skcx_{k+1}) = 0$.
2^o $skcx_k \cap skcx_{k-1} \neq \emptyset \Rightarrow \delta^2(skcx_k, skcx_{k-1}) = 0$.

Proof.

1^o It can be established that $skcx_k \cap skcx_{k+1} \neq \phi$ by definition of a spoke complex. Which implies $\delta^2(skcx_k, skcx_{k+1}) = 0$ as per axiom (**hP3**).
2^o It can be estabilised that $skcx_{k-1} \cap skcx_k \neq \phi$ by the definition of a spoke complex. Which implies $\delta^2(skcx_{k-1}, skcx_k) = 0$ as per axiom (**hP3**)

□

Next, consider a result pertaining to the descriptive Lodato hyper-connectedness(δ^n_Φ).

Theorem 3. *Let K a cell complex equipped with a descriptive hyper-connectedness relation. Let $skcx_{k-1}, skcx_k, skcx_{k+1} \in K$ be spoke complexes in K. Then*

1^o $skcx_k \cap skcx_{k+1} \neq \emptyset \Rightarrow \delta^2_\Phi(skcx_k, skcx_{k+1}) = 0.$
2^o $skcx_k \cap skcx_{k-1} \neq \emptyset \Rightarrow \delta^2_\Phi(skcx_k, skcx_{k-1}) = 0.$

Proof. 1^o It can be established that $skcx_k \cap skcx_{k+1} \neq \emptyset$ by definition of a spoke complex. Suppose $x \in skcx_k \cap skcx_{k+1}$, then $x \in skcx_k \cup skcx_{k+1}$ and $x \in \phi(skcx_k)$, $x \in \phi(skcx_{k+1})$. Hence, $skcx_k \underset{\Phi}{\bigcap} skcx_{k+1}$. From axiom (**hdP3**), this implies $\delta^2_\Phi(skcx_k, skcx_{k+1}) = 0$.

2^o It can be established that $skcx_k \cap skcx_{k-1} \neq \emptyset$ by definition of a spoke complex. Suppose $x \in skcx_k \cap skcx_{k-1}$, then $x \in skcx_k \cup skcx_{k-1}$ and $x \in \phi(skcx_k)$, $x \in \phi(skcx_{k-1})$. Hence, $skcx_k \underset{\Phi}{\bigcap} skcx_{k-1}$. From axiom (**hdP3**), this implies $\delta^2_\Phi(skcx_k, skcx_{k-1}) = 0$.

□

Theorems 2 and 3 give results for spatial($\delta^k = 0$) and descriptive($\delta^k_\Phi = 0$) hyper-connectedness, respectively. Consider next results for sub-complexes that are far either spatially($\delta^k = 1$) or descriptively($\delta^k_\Phi = 1$).

Theorem 4. *Let $(K, \{\delta^n, \delta^n_\Phi\})$ be a relator space equipped with two hyper-connectedness relations and let $skcx_j, skcx_k \in K$ be spoke complexes in the K, where $j, k \in \mathbb{Z}^+$. Then*
1^o $\|j - k\| \geq 2 \Leftrightarrow \delta^2(skcx_j, skcx_k) = 1.$
2^o $\|j - k\| \geq 2 \not\Rightarrow \delta^2_\Phi(skcx_j, skcx_k) = 1.$

Proof. 1^o Since this is a biconditional, we need to prove the implication in both directions. By the definition of spoke complex it can be established that $skcx_k \cap skcx_j \neq \emptyset \Leftrightarrow \|j - k\| \geq 2$. Using a result from (Naimpally & Warrack, 1970, pg. 7), if a space is equipped with a pseudo-metric and $D(A, B) = inf\{d(a, b) : a \in A, b \in B\}$, then $A\delta B$ iff $D(A, B) = 0$. Suppose K is a Euclidean space equipped with the Euclidean metric. It follows that in this triangulation $D(A, B) = 0 iff A \cap B \neq \emptyset$. Thus, $D(skcx_k, skcx_j) = 0$ iff $\|j - k\| < 2$ and $D(skcx_k, skcx_j) \neq 0$ otherwise. Hence, we can conclude that $\|j - k\| \geq 2 \Leftrightarrow \delta^2(skcx_j, skcx_k) = 1$.

2^o It can be established from the definition of the spoke complex that any $\sigma^2 \in K$, that is not in $skcx_k$ but has a non-empty intersection with $skcx_k$ is an element of $skcx_{k+1}$. Thus, it can be established that $skcx_j \cap skcx_k \neq \emptyset$ iff $\|j - k\| \leq 1$. Which means $j \in \{k - 1, k, k + 1\}$. From this we can establish that $skcx_j \cap skcx_k = \emptyset$ if $\|j - k\| \geq 2$. From the definition of $\underset{\Phi}{\cap}$, it follows that $A \cap B \Rightarrow A \underset{\Phi}{\cap} B$, and $A \underset{\Phi}{\cap} B \not\Rightarrow A \cap B$. Thus, it is possible that $A \underset{\Phi}{\cap} B$ eventhough $A \cap B = \phi$. Thus, it is still possible that $skcx_j \underset{\Phi}{\cap} skcx_k \neq \emptyset$ even if $\|j - k\| \geq 2$. From axiom (**hdP3**), we can conclude that, $\delta^2_\Phi(skcx_j, skcx_k) = 0$ even if $\|j - k\|$. Hence proved.

□

The notion of proximity in a space can be defined using a function. Let us cosntruct a function which quantifies the proximity of a subset to the nucleus of a MNC in the triangulation.

Definition 1. *Let K be a triangulation, $d \subset K$ be the nucleus and $A, skcx_k \subset K$. Then, $\mu_d(A) : K \to \mathbb{Z}^+$ is a function satisfying*

$$A \subset skcx_k \Leftrightarrow \mu_d(A) = k.$$

We can use this function to quantify the proximity between pairs $\sigma^2 \in K$ by using the MNC as a reference point.

Definition 2. *Let A, B are two $\sigma^2 \in K$, μ_d is a function as defined in def. 1. We can define*

$$\mu_d(A, B) = \|\mu_d(B) - \mu_d(A)\|.$$

It can be shown that $\mu_d(x, y)$ is a pseudo-metric.

Theorem 5. *Let K be a triangulation of a finite, bounded planar region, $A, B, C \in K$ be σ^2, and let $d \subset K$ be the MNC. We can define a function $\mu_d(A, B)$ as per def. 2. Then*
1^o $\mu_d(A, A) = 0$.
2^o $\mu_d(A, B) = \mu_d(B, A)$.
3^o $\mu_d(A, C) \leq \mu_d(A, B) + \mu_d(B, C)$.
Hence, $\mu_d(A, B)$ is a pseudo-metric.

Proof. 1^o is true by definition, since $\mu_d(A, A) = \|\mu_d(A) - \mu_d(A)\| = 0$.
2^o is true by definition, since $\mu_d(A, B) = \|\mu_d(B) - \mu_d(A)\| = \|\mu_d(A) - \mu_d(B)\| = \mu_d(B, A)$
3^o To prove this, consider the following two cases. First, let B, C are in the same spoke complex and A in a different complex, $B, C \in skcx_k$, and $A \in skcx_j$. Then it is easy to see that $\mu_d(A, C) = \mu_d(A, B) + \mu_d(B, C)$, as $\mu_d(B, C) = 0$, $\mu_d(A, B) = \mu_d(B, A) = \|j - k\|$.
For the second case, let A, B, C be in different spoke complexes, where $A \in skcx_j$,$B \in skcx_k$ and $C \in skcx_l$. For simplicity, let us divide this into two subcases. Let us begin with $j < k < l$. It can be seen that $\mu_d(A, C) = \mu_d(A, B) + \mu_d(B, C)$, as $\mu_d(A, C) = \|l - j\|$, $\mu_d(A, B) = \|k - j|$ and $\mu_d(B, C) = \|l - k\|$. The second subcase is $j < l < k$. It can be seen that $\mu_d(A, C) < \mu_d(A, B) + \mu_d(B, C)$, as $\mu_d(A, C) = \|l - j\|$, $\mu_d(A, B) = \|k - j|$ and $\mu_d(B, C) = \|l - k\|$. Hence, we have proved that $\mu_d(A, C) \leq \mu_d(A, B) + \mu_d(B, C)$.

□

It can be established that $\mu_d(A, B)$ is not a metric, since $\mu_d(A, B) = 0$ for any two distinct σ^2 in the same spoke complex $A, B \in skcx_k$, as per def. 1. A spoke complex is a subcomplex of the original triangulation K. It is important to note that as per the def. 1, every $\sigma^2 \in skcx_k$ has the same proximity, as quantified by μ_d, to the MNC. Moreover, the $\sigma^2 \in skcx_k$ have $\mu_d = 0$ with each other. Let us define some new notions using the function μ_d.

Definition 3. *Let K be a CW complex, μ_d be the function as per def. 1. We only relax the codition that d is a nucleus of an MNC and let it be any arbitrary $\sigma \in K$. Then*

$$K^n_{\mu,d} = \{\sigma^2 : \sigma^2 \in K \, and \, \mu_d(\sigma^2) = n\}$$

is a n-proximal subcomplex of K w.r.t base point d.

We can term all the n-proximal subcomplexes as *iso-proximal complexes*, since all of their elements the same proximity, as quantified by μ_d to the base point. It is also important to note the following result.

Theorem 6. *Let K be a triangulation, $d \subset K$ be the nucleus and $skcx_k \in K$ be the k-spoke complex. Then,*

$$skcx_k \iff K^k_{\mu,d}$$

Proof. This follows directly from defs. 1 and 3. □

We specify the notation for a cycle in a triangulation. Suppose $a, b, c \in K$ are three vertices, then (abc) is a cycle such that there is a path from a back to a, passing through b and c. Moreover, $cntr(a)$ represents the centroid of set a. Let us define the notion of an iso-proximal cycle using the function μ_d.

Definition 4. *Let K be a CW complex, μ_d be the function from def. 1. We relax the condition that d is the nucleus of a MNC and let it be an arbitrary $\sigma \in K$. Let us first generate an index set of the $\sigma^2 \in K^k_{\mu,d}$ as follows*

$$\mathcal{K} = \{k_i : k_i = \sigma^2 \in K^k_{\mu,d}, k_i = k_j \iff i = j, i \in \mathbb{Z}^+\}.$$

Now, using this index set we can define the notion

$$cyc^n_{\mu,d} = \{(a_1 a_2 \cdots a_n) : a_i = cntr(k_i)\ s.t.\ k_i \in \mathcal{K}\}.$$

Here, $cyc^n_{\mu,d}$ is a $n-$proximal cycle of K relative to the base point d.

Similar to the notion of n-proximal complex, a n-proximal cycle can be termed an iso-proximal cycle. Next, consider the following result.

Theorem 7. *Let K be a triangulation, $d \subset K$ be the nucleus and $mcyc_k d$ be the maximal k-cycle. Then*

$$mcyc_k d \iff cyc^k_{\mu,d}.$$

Proof. A maximal k-cycle, $mcyc_k$, is a simple closed path connecting the centroids of all the $sk_k \in K$. Comparing this with Def. 4, it follows that maximal k-cycle is a $k-$proximal cycle. □

To help clarify the concepts we have introduced, we give an example.

Example 3. *We illustrate the spke complexes in a stock digital image peppers.png in MATLAB®. Now consider theorem 6 stating the equivalence between the k^{th} spoke complex and $k-$proximal cycle w.r.t. nucleus as the base point. Thus, $skcx_1$ shown in yellow is $K^1_{\mu,d}$, $skcx_2$ (blue) is $K^2_{\mu,d}$, $skcx_3$ (green) is $K^3_{\mu,d}$ and $skcx_4$ (orange) is $K^4_{\mu,d}$. Let us now move on to theorem 7, which states that k^{th} maximal centroidal cycle is the $k-$proximal cycle w.r.t. nucleus as the base point. Thus, $mcyc_1$ shown in blue is the $cyc^1_{\mu,d}$, $mcyc_2$(red) is $cyc^2_{\mu,d}$, $mcyc_3$(orange) is $cyc^3_{\mu,d}$ and $mcyc_4$(indigo) is $cyc^4_{\mu,d}$. Now that we have seen how the iso-proximal complexes and cycles are defined in digital images, let us look at a closely associated concept in meteorology. It is the conept of an isobar, which is a line connecting points with the same barometric pressure.*

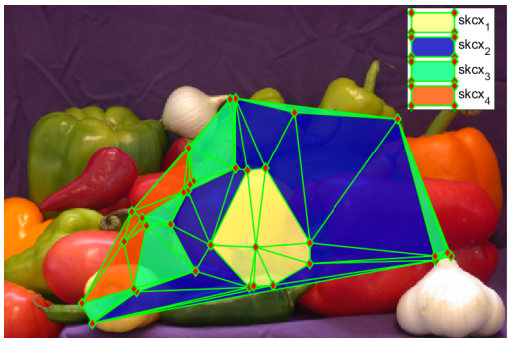

3.1: $skcx_k$ in digital image

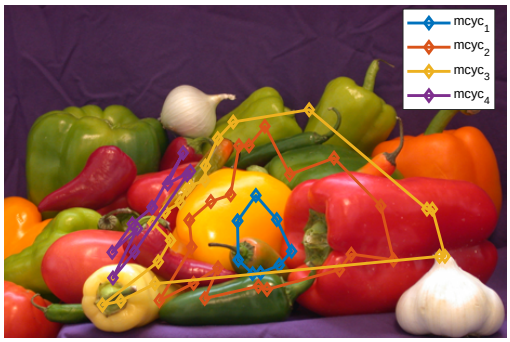

3.2: $mcyc_k$ in digital image

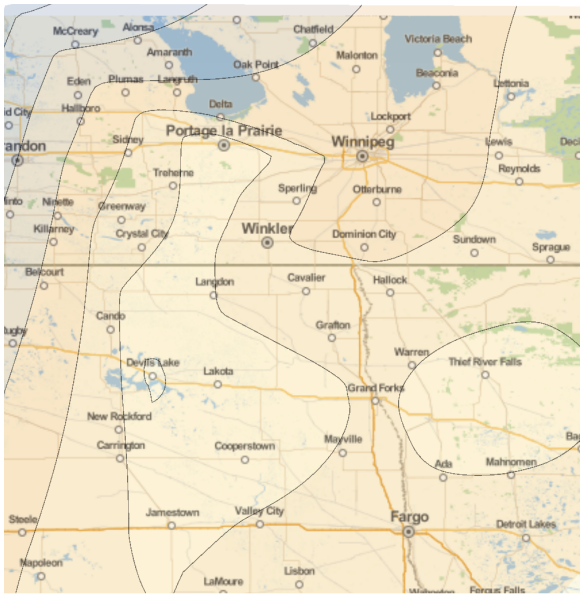

3.3: Isobars in Weather Maps

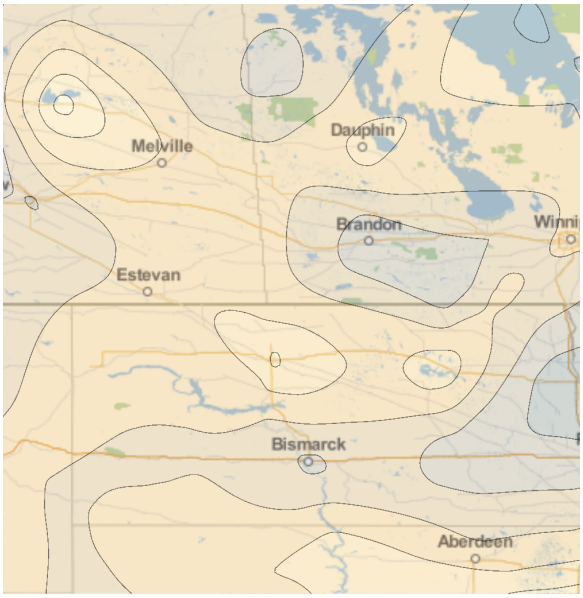

3.4: Isotherms in Weather Maps

Figure 3: This figure illustrates the concepts of iso-proximal complexes and cycles. Fig. 3.1 shows the $skcx_k$, each of which is an iso-proximal complex. Fig. 3.2 shows $mcyc_k$, each of which is an iso-proximal cycle. Fig. 3.3 is an example of isobars in weather map, generated using Mathematica. Fig. 3.4 is an example of isotherms in weather map, generated using Mathematica.

Replace μ in the definition of $cyc^k_{\mu,d}$, which is a function that measures proximity w.r.t. point d, with the function that defines barometeric pressure over the surface of earth. We can then get isobars in a region around Winnipeg using Mathematica as shown in Fig. 3.3. Each of the black lines connects regions with similar pressure. The value of barometric pressure is different for each line. Again in the case of isotherms, we have lines connecting regions with identical tempratures. Next, we can obtain a similar effect by replacing μ with a function that defines air temperature over the surface of earth. Isotherms in the region around Winnipeg are shown in Fig. 3.4. These are also generated using Mathematica. Similarly, each of the black lines corresponds to a different temprature. The regions on each line have same value of air temprature. ■

4. Descriptve Frame Recurrence Diagrams

This section introduces what are known as descriptive frame recurrence diagrams derived from triangulated video frames. For construction of the Delaunay trianglation of video frames, we use hole based keypoints. A hole is defined as a region of constant intensity in a digital image. For this purpose, we use the gradient magnitude for detection and filter out small holes based on the number of pixels contained in them. The process is detailed in Alg. 1. These keypoints are used

Algorithm 1: Hole based Keypoints

Input : digital image *img*, Horizontal filter radius r_x, Vertical filter radius r_y, Hole threshold t, Number of holes n_{hole}

Output: Hole locations $\mathscr{K}_{holes}$

$g :=$ *empty matrix*;
foreach *pixel* $\in$ *img* **do**
  $g(i, j) \leftarrow$ *Gradient Magnitude at* (i, j);
$g :=$ *set all values of* $g < t$ *to* 1 *and rest to* 0;
$g \mapsto$ *connected components*;
connected components $\mapsto$ *size in terms of pixels*;
/* arrange in descending order w.r.t. size in terms of pixels */;
connected components $\mapsto$ *arranged connected components*;
hole $\leftarrow$*first* n_{hole} *arranged connected components*;
hole $\mapsto$ *centroids*;
$\mathscr{K}_{holes} \leftarrow$ *centroids*;

to generate a triangulation, in which the spoke complexes and the maximal centroidal vortices are identified. The process of detecting the spoke complexes starts with the identification of MNCs. The nucleus($skcx_0$) in a triangulation are the vertices that are common to the greatest number of triangles. The nuclei along with the repective triangles containing them are the MNCs($skcx_1$). The triangles that are excluded in $skcx_i$ for $i = 0, 1$, and share interesections(vertices, edges) with $skcx_1$ are included in the $skcx_2$. $skcx_k$ for any $k > 2$ can be constructed in a similar fashion. The process stops when all the triangles in the triangulation have been assigned to a particular level k in the spoke complex. It is to be noted that we have separate $skcx_k$ for each of the nuclei.

The construction of centroidal maximal centroidal cycles follows from this. The $mcyc_k$ is a closed simple path that connects the centroids of triangles included in $skcx_k$. There is a slight problem regarding the arrangements of centroids so as to form a non-intersecting cycle. For this we caluclate the centroid of vertices in a particular $mcyc_k$, represented as $cntr_{cyck} = (cntr^x_{cyck}, cntr^y_{cyck})$. Then for each vertex $v_i = (v^x_i, v^y_i) \in mcyc_k$ calculate arctan $\frac{v^y_i - cntr^y_{cyck}}{v^x_i - cntr^x_{cyck}}$. Going through the vertices in order of ascending values of this quantity results in a simple closed path. The collection of all the $mcyc_k$ is the maximal centroidal vortex.

In Theorems 6 and 7, we have established that each of the spoke complexes is a cell complex is an iso-proximal complex and maximal centroidal cycles are iso-proximal cycles. These structures encode the spatial proximity of sub-regions in a triangulated finite, bounded planar region. This is an alternate way to study the topology or the shape of a space. Traditionaly, the interior of a shape is considered to have binary nature. It is either empty or nonempty, which paves the way for shape interiors with subregions that are holes. This is a narrow view which is ill-suited to the study of digital images which have a rich interior that is instrumental in understanding and analysis. An earlier attempt at overhauling the classical methods of homology(classification of shapes based on the holes) was taken up in (Ahmad & Peters, 2018). Using the notion of iso-proximal cycles and complexes the description of a shape interior can be fused with a consideration of spatial proximities.

Next, we introduce structures to integrate proximity structure of triangulation with the description of interiors. For this purpose, we introduce descriptive maximal centroidal cycles. A fibre bundle is a structure (E, B, π, F), where $\pi : E \to B$ is a continuous surjection, E is the *total space*, B is the *base space* and $F \subset E$ is the *fiber*. Using this framework we can define two different structures. The first of these is

Definition 5. *Let $mcyc_k$ be a maximal k-cycle, $skcx_k$ a k−spoke complex in a triangulation CW complex K. Let us define a function,*

$$\phi_{vrt} : 2^K \to \mathbb{R}^n,$$
$$a \mapsto \begin{cases} \phi_{vrt}(a) & if\, a = cntr(\triangle \in skcx_k), \\ 0 & otherwise, \end{cases}$$

Then the descriptive maximal k-cycle (denoted by $mcyc^{\phi}_k$) is a fiber bundle $(mcyc^{\phi}_k, mcyc_k, \pi, \phi_{vrt}(U))$, where $U \subset mcyc_k$.

A variant of the above is

Definition 6. *Let $mcyc_k$ be a maximal k− cycle, $skcx_k$ be a k−spoke complex in a triangulation K. Let us define a function,*

$$\phi_{avg} : 2^K \to \mathbb{R}^n$$
$$a \mapsto \begin{cases} \frac{\sum \phi(a)}{|a|} & if\, a = cntr(\triangle \in skcx_k), \\ 0 & otherwise, \end{cases}$$

Then the region descriptive maximal k-cycle ($mcyc_k^{\bar{\phi}}$), is a fiber bundle ($mcyc_k^{\bar{\phi}}, mcyc_k, \pi, \phi_{vrt}(U)$), where $U \subset mcyc_k$.

The two proposed structures, namely the descriptive($mcyc_k^{\phi}$) and region descriptive maximal cycle($mcyc_k^{\bar{\phi}}$), differ only slightly. The basic idea behind these structures is that each vertex in a $mcyc_k$ corresponds to a trinagle in the $skcx_k$. We have established via Thm. 6 that each of the triangles in a $skcx_k$ has the same proximity to the nucleus. We have also established vis Thm. 7 that each of the vertices in a $mcyc_k$ is the centroid of a triangle in $skcx_k$. Thus, both $skcx_k$ and $mcyc_k$ encode the spatial proximity of the triangulation.

Next, we choose $mcyc_k$ as the base space and then assign to each vertex a description using the probe functions ϕ_{vrt} or ϕ_{avg}. The only differennce between the two probes is that ϕ_{vrt} assigns to a vertex the description at centroid of the corresponding triangle in $skcx_k$, while ϕ_{avg} assigns the average description of all the subregions(pixels) of the triangle. These descriptions can be arranged in the form of a vector for each of the $mcyc_k$ or combine all into a single vector. The basic feature that we will be using in this study is wavelength,λ. It is a nonlinear function of hue. The first step in the calculation of λ is the conversion of RGB image to HSV (Hue Saturation Value). Then we transform the hue channel(h) according to the following equation which is an approximation of the nonlinear mapping.

$$\lambda(i,j) = \begin{cases} 435nm & \text{if } h(i,j) > 0.7483, \\ \frac{-(h(i,j)-2.60836)}{0.004276} & otherwise. \end{cases} \tag{4.1}$$

Here we assume that the hue values are scaled between [0, 1]. The wavelengths caluclated by this equation (measured in nanometers nm, *i.e.*, 10^{-9} meter) are limited to the range $[435nm, 610nm]$.

A consideration of hue wavelength gives a useful feature vector useful in the study of shapes in video frames. The i^{th} image(frame) is represented as $\mathcal{V}_i$. Tracking similar frames in a video is important. We use the framework of descriptive similarity with the two probe functions defined in Defs. 5,6. To discuss regarding similarity of frames we define a feature vector,

$$\eta_\phi(\mathcal{V}_i) = \{\frac{\sum\limits_{\forall \triangle \in skcx_k} \phi(mcyc_k(\mathcal{V}_i))}{|skcx_k|} : \text{for } k \in \mathbb{Z}^+, \text{and } \phi = \phi_{avg} \text{ or } \phi_{vrt}\}, \tag{4.2}$$

where $|skcx_k|$ is the number of triangles in $skcx_k$ and $mcyc_k(\mathcal{V}_i)$ is a maximal centroidal cycle in frame i of the video. Two frames are similar if,

$$\delta^2_\Phi(\mathcal{V}_i, \mathcal{V}_j) = 0 \iff \|\eta_\phi(\mathcal{V}_i) - \eta_\phi(\mathcal{V}_j)\|_2 \leq th, \tag{4.3}$$

where th is a suitable threshold empirically determined.

Since it is possible for an image to have multiple maximal vortices, we compute the value of ϕ for each vortiex and then compare the value for all the possible combinations. If any of the multiple vortices in an image are similar to any in the other image, then these frames are said to be similar. Let us plot $\delta^2_\Phi(V_i, V_j)$ for $i, j = 1, \cdots, |\mathcal{V}|$, where $|\mathcal{V}|$ is the number of frames in the video. As δ^2_Φ is a binary relation we only mark the locations for which $\delta^2_\Phi(\mathcal{V}_i, \mathcal{V}_j) = 0$. Moreover, due to the symmetry of Euclidean distance($\|\cdot\|_2$}) we can ignore the lower half below the diagonal.

Moreover, as each frame is similar to itself, the diagonal is always marked. This leads to what we call a *descriptive frame recurrence diagram* and mark it as $\mathcal{R}_\Phi(\mathcal{V}, th)$ for video $\mathcal{V}$ and threshold th. We present a formal definition of the descriptive frame recurrence diagram.

Definition 7. *Let $\mathcal{V}$ be a video η_ϕ be a feature vector as defined in Eq. 4.2 . Then,*

$$\mathbb{R}_\Phi(\mathcal{V}, th) = \{(i, j) : \|\eta_\phi(\mathcal{V}_i) - \eta_\phi(\mathcal{V}_j)\|_2 \leq th, j \geq i \text{ and } i, j = 1, \cdots, |\mathcal{V}|\},$$

where $th \in \mathbb{R}^+$ and $|\mathcal{V}|$ is the number of frames in the video $\mathcal{V}$. The set $\mathcal{R}_\Phi(\mathcal{V}, th)$ is the descriptive frame recurrence diagram.

We combine all the tools presented above in a framework for video processing, illustrated in Fig. 4. Calculation of $skcx_k$ and $mcyc_k$ for all the frames of a video is the starting step. Once, we have the $mcyc_k$ we calculate $\eta_\phi(\mathcal{V}_i)$ as defined in Eq. 4.2. For this step we use wavelength,λ defined in Eq. 4.1, as the probe function ϕ. The last step is to calculate the recurrance diagram $\mathcal{R}_\Phi(\mathcal{V}, th)$ as defined in Def. 7. Thus, for every frame $\mathcal{V}_i$ a recurrance diagram tells values of $j > i$, such that $\delta^2_\Phi(\mathcal{V}_i, \mathcal{V}_j) = 0$.

5. Application of Descriptive Frame Recurrence Diagrams

This section introduces an application of descriptive frame recurrence diagrams in terms of the occurrence of similar frames in a video. In this section, we will present a pair of frames detected as similar using each of the probe functions defined in Defs. 5,6. Then we finish the section with a pair frames that are not similar for both probe functions.

We start the discussion with the vertex-based probe function defined in Def. 5. In this probe as discussed in Sec. 4, we only use the value of probe function at the vertices of cycles(centroids of triangles in spoke complexes). The feature that we are interested in is the wavelength as calculated using the Eq. 4.1. The results are displayed in the Fig. 5.

We calculate the descriptive frame recurrence diagram for the video $\mathcal{V}$. It is represented as $\mathcal{R}_\Phi(\mathcal{V}, th)$ and is shown in Fig. 5.1. For this study we set $th = 5$. It can be seen that apart from the diagonal only four other points show up in $\mathcal{R}_\Phi(\mathcal{V}, th)$. Since every frame is similar to itself we only look at the points apart from the diagonal. We select a pair of frames$((15, 87))$ marked with a red circle in Fig. 5.1. We display frame 15 in Fig. 5.2 and frame 87 in Fig. 5.3.

Next we display the $skcx_k$ and corresponding $mcyc_k$, $k = 1, \cdots, 4$, for both the frames. Figs. 5.4, 5.5 display $skcx_1$ and corresponding $mcyc_1$ for frame 15 and 87 respectivly. It can be seen that both the $skcx_1$ and $mcyc_1$ are identical for both the frames. $skcx_2$ and $mcyc_2$ are also identical for both the frames as shown in Figs. 5.6,5.7. The $skcx_3$ and corresponding $mcyc_3$ for frame 15 is in Fig. 5.8, and $skcx_3$ and $mcyc_3$ for frame 87 is illustrated in Fig. 5.9. The $skcx_3$ and $mcyc_3$ are slightly different. Figs. 5.10,5.11 show the $skcx_4$ and $mcyc_4$ for both the frames. It is evident from the figures that spoke complex at level 4 and the corresponding maximal centroidal cycles differ slightly for the frames.

Now that we have seen the $mcyc_k$ for both the frames, let us comapre the values of ϕ_{vrt} for different cycles across the two frames. For ease of comparison we take the average value of ϕ_{vrt} calculated at all the vertices in an $mcyc_k$ for a particular k. We plot these values as a bar graph

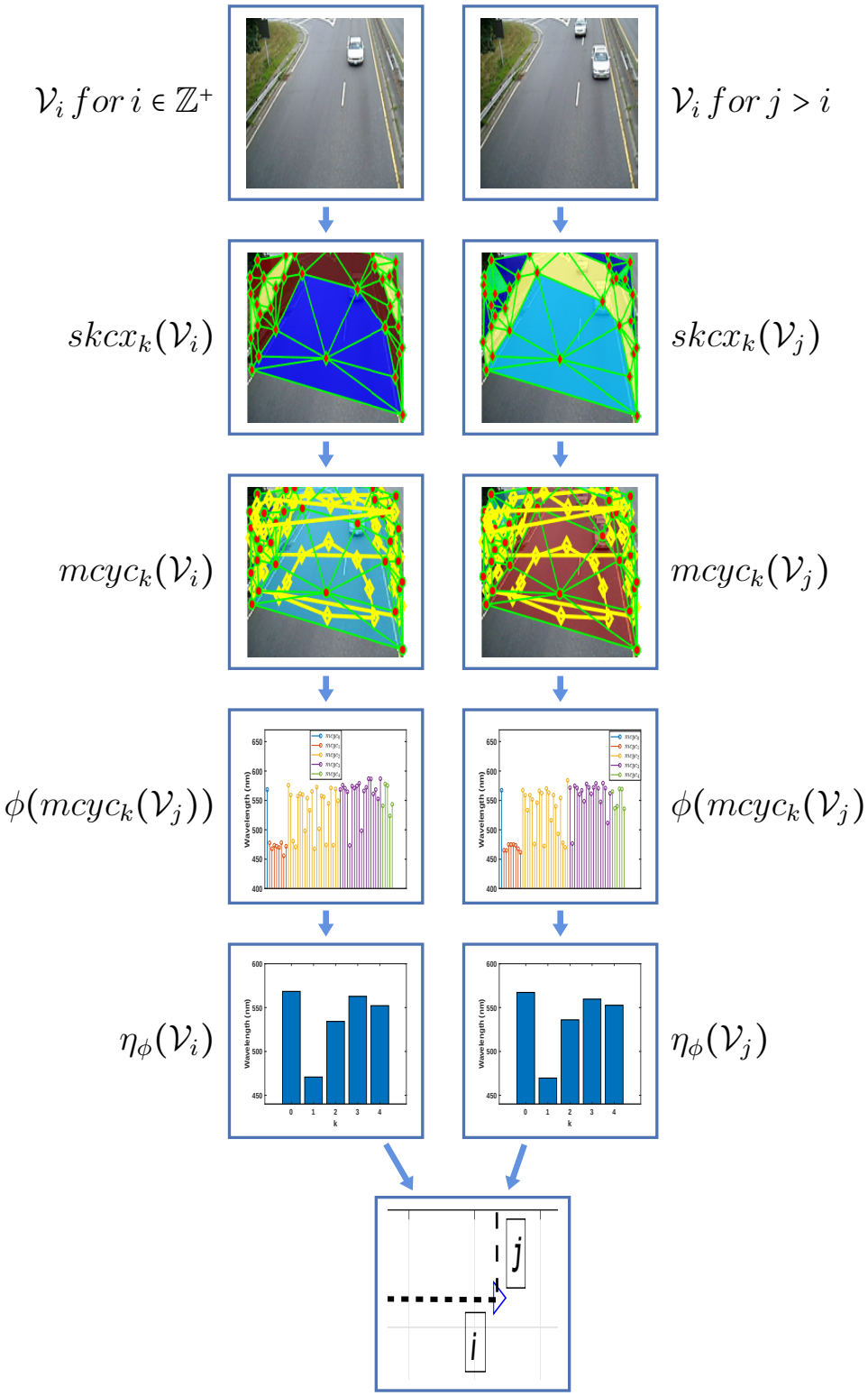

Figure 4: This flow diagram illustrates the methodology for constructing a descriptive frame recurrance diagram, $\mathcal{R}_\Phi(\mathcal{V}, th)$. Repeating thsi process for all valid pairs of (i, j), such that $i = 1, \cdots, |\mathcal{V}|$ and $j > i$. Here, $\mathcal{V}$ represents the number of frames in the video.

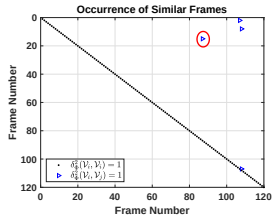

5.1: Descriptive Frame Recurrance

5.2: Frame 1

5.3: Frame 2

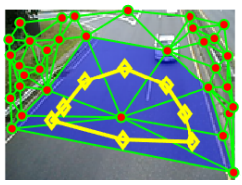

5.4: $skcx_1$ and $mcyc_1$ in Frame 1

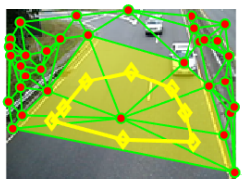

5.5: $skcx_1$ and $mcyc_1$ in Frame 2

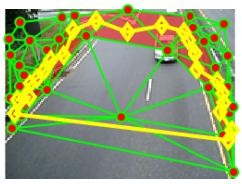

5.6: $skcx_2$ and $mcyc_2$ in Frame 1

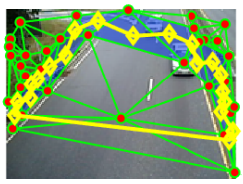

5.7: $skcx_2$ and $mcyc_2$ in Frame 2

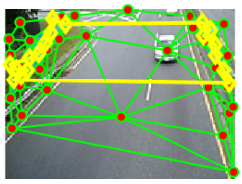

5.8: $skcx_3$ and $mcyc_3$ in Frame 1

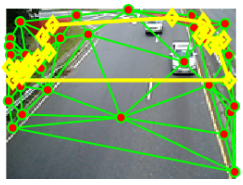

5.9: $skcx_3$ and $mcyc_3$ in Frame 2

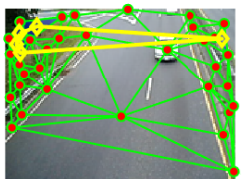

5.10: $skcx_4$ and $mcyc_4$ in Frame 1

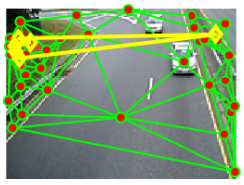

5.11: $skcx_4$ and $mcyc_4$ in Frame 2

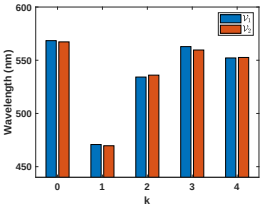

5.12: Mean Wavelengths for both images

Figure 5: This figure illustrates the application of the framework developed in sec. 4. In this illustration we use the values of wavelengts at centroids only. Fig. 5.1, represents the descriptive frame recurrance diagram. The red circle annotates the frame pair being analyzed. Fig. 5.2,5.3 are the frames that have been detected as descriptivly similar. Figs. 5.4,5.6,5.8,5.10 represent $skcx_k$ and corresponding $mcyc_k, k = 1, \cdots, 4$ for frame in Fig. 5.2. Figs. 5.5,5.7,5.9,5.11 represent $skcx_k$ and corresponding $mcyc_k, k = 1, \cdots, 4$ for frame in Fig. 5.3. Figs. 5.12 represents the average wavelengts calculated at each spoke level k. $skcx_0$ and $mcyc_0$ are the nucleus. The frames are similar in terms of these values as can be seen in this figure.

comparing the frames in Fig. 5.12. It can bee seen that values almost identical for the different $mcyc_k$ across the frames. We conclude that $\delta^2_\Phi(\mathcal{V}_{15}, \mathcal{V}_{87}) = 0$. Most noticable difference occurs for $k = 3$. It must be noted that both the images shown in Fig. 5.2,5.3 have multiple vortices.

In the Fig. 5 we only show cycles across the frames that were detected as being descriptivly similar(δ^2_Φ). It is in teresting to note that frame 15 and 87 are almost identical apart from the fact that later has two cars. The position of cars, their shape and color are almost identical. The fact that location, shape and the description of these vortices are similar is due to the similarity in images.

Next, consider the case of ϕ_{avg}, region based probe defined in 6. The result for this method are displayed in Fig. 6. The structure of the figure is similar to one adopted for Fig. 5. We start by showing the descriptive frame recurrence diagram $\mathcal{R}_\Phi(\mathcal{V}, th)$ in Fig. 6.1. The value of $th = 5$ is the same for this study also. It can be noted that apart from the diagonal there are eight other points in the diagram, representing a pair of frames that is descriptivly similar. The number of off-diagonal points was only four for the case(Fig. 5) where neighborhood was not used. This can be easily explained as the ϕ_{vrt} only takes into account the value of feature at a single point(the centroid of triangles).

The value at a single pixel in an image can vary due a number of reasons e.g. quantization errors, noise, motion artifacts and sudden changes in illumination at the scene. Thus there is a chance that similar frames can be detected as disimilar when using ϕ_{vrt}. When we use the neighborhood, noise and illumination effects cancel due to averaging over a region. This can also lead to two different frames being classified as similar if the changes are small enough to be destroyed in averaging.

Consider next a marked as a red circle in Fig. 6.1, namely, the frame 63 shown in Fig. 6.2 and the frame 110 in Fig. 7.3. There are some similarities and differences in the frames. Frame 63 has three cars while the frame 110 has only one car. The car in frame 110 is similar to one of the cars in frame 63 but not identical and it is in the different lane.

This pair of frames have similar vortices due to the fact that we are looking at wavelengths in a region as opposed to at a point. The cars are black, the same color as the road, which results in their being detected as similar in terms of wavelength averaged over the spoke triangles. Let us look at the $skcx_k$ and the corresponding $mcyc_k$ for both the frames. The Figs. 6.4,6.6,6.8,6.10,6.12 illustrate $skcx_k$ and $mcyc_k$ for $k = 1, \cdots, 5$, in frame 63(Fig.). Figs. 6.5,6.7,6.9,6.11,6.13 represent $skcx_k$ and $mcyc_k$ for frame 110. We can observe that all the spokes vary slightly interms of structure.

This structural vairation is due to the slight difference in the triangulation of frames. The reason that spoke lie in almost the same area accounts for the similarity. The black cars occurs in different spoke levels but their color is almost similar to color of road thus the difference is not registered when we average over the spoke. We ahve seen in Eq. 4.1 that the wavelength is a fucntion of hue or the color. This fact is further established when we look at the average wavelengths for each of the $mcyc_k$ and compare them across the two frames in Fig. 6.14.

There are slight difference in the values for each value of k and the overall difference is smaller than the threshold. Hence $\delta^2_\Phi(\mathcal{V}_{63}, \mathcal{V}_{110}) = 0$. This is an example of the flexibility yielded by the neighborhood based probe function(ϕ_{avg},Def. 6) yields as compared to the vertex based probe(ϕ_{vrt},Def. 5). It can be seen that frames detected as similar by ϕ_{vrt} are almost identical in all

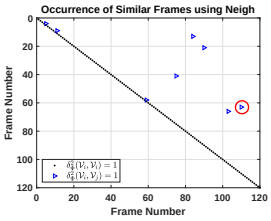

6.1: Descriptive Frame Recurrance

6.2: Frame 1

6.3: Frame 2

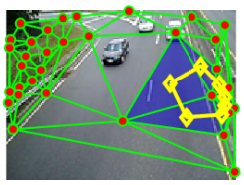

6.4: $skcx_1$ and $mcyc_1$ in Frame 1

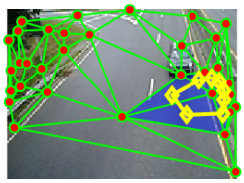

6.5: $skcx_1$ and $mcyc_1$ in Frame 2

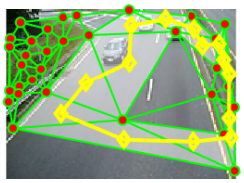

6.6: $skcx_2$ and $mcyc_2$ in Frame 1

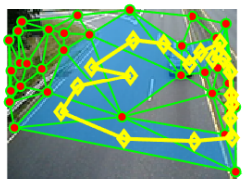

6.7: $skcx_2$ and $mcyc_2$ in Frame 2

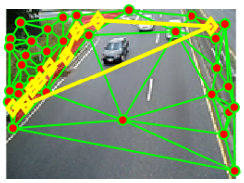

6.8: $skcx_3$ and $mcyc_3$ in Frame 1

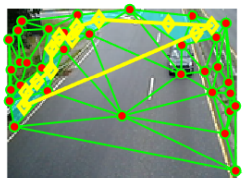

6.9: $skcx_3$ and $mcyc_3$ in Frame 2

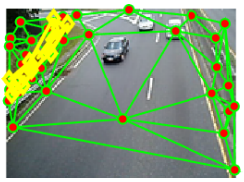

6.10: $skcx_4$ and $mcyc_4$ in Frame 1

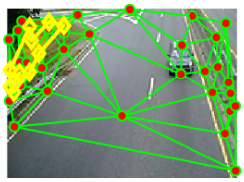

6.11: $skcx_4$ and $mcyc_4$ in Frame 2

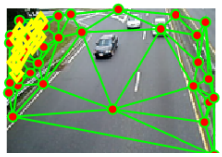

6.12: $skcx_5$ and $mcyc_5$ in Frame 1

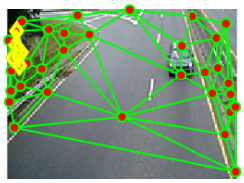

6.13: $skcx_5$ and $mcyc_5$ in Frame 2

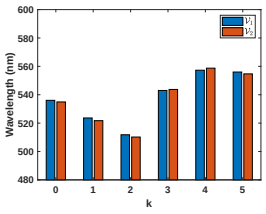

6.14: Mean Wavelengths for both images

Figure 6: This figure illustrates the application of framework developed in sec. 4. In this illustration we use the values of wavelengts averaged over the spoke triangles(neighborhoods). Fig. 6.1, represents the descriptive frame recurrance diagram. The red circle annotates the frame pair being analyzed. Fig. 6.2,6.3 are the frames that have been detected as descriptivly similar. Figs. 6.4,6.6,6.8,6.10,6.12 represent $skcx_k$ and corresponding $mcyc_k, k = 1, \cdots, 5$ for frame in Fig. 6.2. Figs. 6.5,6.7,6.9,6.11,6.13 represent $skcx_k$ and corresponding $mcyc_k, k = 1, \cdots, 5$ for frame in Fig. 6.3. Figs. 6.14 represents the average wavelengts calculated at each spoke level k. $skcx_0$ and $mcyc_0$ are the nucleus. The frames are similar in terms of these values as can be seen in this figure.

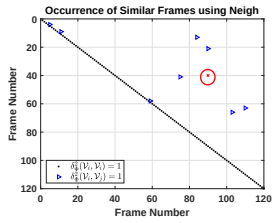

7.1: Descriptive Frame Recurrance

7.2: Frame 1

7.3: Frame 2

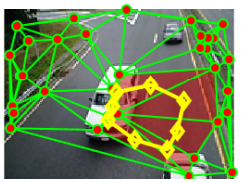

7.4: $skcx_1$ and $mcyc_1$ in Frame 1

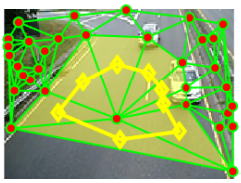

7.5: $skcx_1$ and $mcyc_1$ in Frame 2

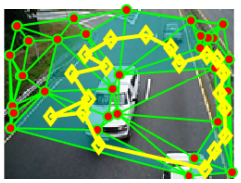

7.6: $skcx_2$ and $mcyc_2$ in Frame 1

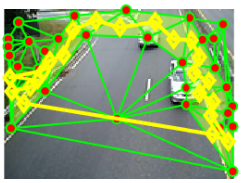

7.7: $skcx_2$ and $mcyc_2$ in Frame 2

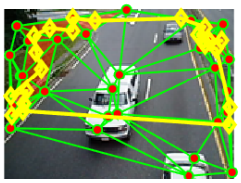

7.8: $skcx_3$ and $mcyc_3$ in Frame 1

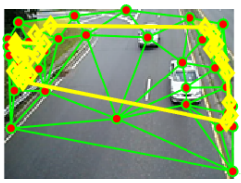

7.9: $skcx_3$ and $mcyc_3$ in Frame 2

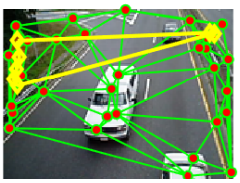

7.10: $skcx_4$ and $mcyc_4$ in Frame 1

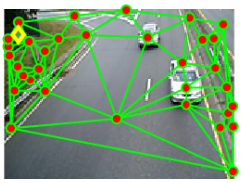

7.11: $skcx_4$ and $mcyc_4$ in Frame 2

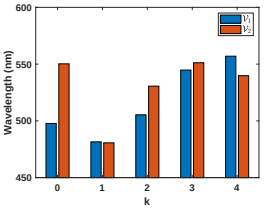

7.12: Mean Wavelengths for both images

Figure 7: This figure illustrates the application of framework developed in sec. 4. In this illustration we display two frames which are dissimilar as none of the vortices are descriptivly similar. Fig. 7.1, represents the descriptive frame recurrance diagram. The red circle and cross annotates the frame pair being analyzed. Fig. 7.2,7.3 are the frames that have been detected as descriptivly not similar. Figs. 7.4,7.6,7.8,7.10 represent $skcx_k$ and corresponding $mcyc_k, k = 1, \cdots, 4$ for frame in Fig. 7.2. Figs. 7.5,7.7,7.9,7.11 represent $skcx_k$ and corresponding $mcyc_k, k = 1, \cdots, 4$ for frame in Fig. 7.3. Figs. 7.12 represents the average wavelengts calculated at each spoke level k. $skcx_0$ and $mcyc_0$ are the nucleus. The frames are not similar due to marked difference in these values as can be seen in this figure.

respects as shown in Fig. 5. The frames detected as similar by ϕ_{avg} have matching aspects such as containing the car of same color and similar background(as the camera position is fixed) but are also different in terms of the location and number of cars.

In addition to resulting from the flexibility due to ϕ_{avg}, it is also necessary to point out its extents. Let us look at a pair of frames that have been marked as dissimilar by both ϕ_{avg} and ϕ_{vrt}. The pair of frames is $(40, 90)$ and the results are displayed in Fig. 7. The pair of frames has been marked by a red cross and circle in $\mathcal{R}_\Phi(\mathcal{V}, th)$ as shown in Fig. 7.1. The threshold value is the same as previous experiments, *i.e.*, $th = 5$.

Consider, first Figs. 7.2, 7.3 to illustrate frame 40 and 90 respectively. It can be observed that the frames are very different in terms of the number and location of cars. This was also the case with Fig. 6, but the frames were detected as similar. In this case there were also cars with similar appearance (the white jeep and white sedan), but the size difference and the location of jeep forces

a lot of keypoints to the center of frame 40. In contrast to this, the keypoints are distributed near the edges with a single point in the middle. Delaunay triangulation thus forces the nucleus to that point and hence the MNC also to the centre. This significant change in the location of the keypoints results in a significant change in structure of the triangulation for both frames.

Now let us move on to the $skcx_k$ and the $mcyc_k$ for both the frames. Figs. 7.4, 7.6, 7.8, 7.10 represent the $skcx_k$ and $mcyc_k$ for $k = 1, \cdots, 4$ in frame 40(Fig. 7.2). Figs. 7.5, 7.7, 7.9, 7.11 represent the $skcx_k$ and $mcyc_k$ for $k = 1, \cdots, 4$ in frame 90(Fig. 7.3). We can see that all the $skcx_k$ and the corresponding $mcyc_k$ have a different structure. Moreover, it is important to note which features of the image lie in the different spokes for each of the frames. Let us first look at the comparison of average wavelengths for the differnet $mcyc_k$. This is presented in Fig. 7.12 for both the frames. It is evident from the bar graph that the major difference lies in $mcyc_0, mcyc_2$ and $mcyc_4$.

Let us now examine the reasons for this difference. As has been established in the paper that when using the neighborhood based probe(ϕ_{avg}) we are not only looking at the vertices in $mcyc_k$ but we are looking at the triangles corresponding to the vertices. Thus, ineffect we are looking at the corresponding $skcx_k$. It must also be noted that $skcx_0$ is the nucleus thus a single point. If we look at Fig. 7.4(frame 40) we can see that the nucleus lies on the bonnet of white jeep, while the nucleus for frame 90, as shown in Fig. 7.4, lies on the black road. As wavelength is a function of the hue(color) as depicted by Eq. 4.1, this explains the difference in average wavelength for $mcyc_0$. If we look at the $skcx_2$ for frame 40 as shown in Fig. 7.6, it can be seen that majority of the areas are black road and a small portion of white car. While for frame 90, shown in Fig. 7.7, most of the regions in $skcx_2$ are the white cars and the green grass. This results in the difference in average wavelength for $skcx_2$ as observed in Fig. 7.12.

With respect to the difference in $skcx_4$, it can be seen that in frame 40, as shown in Fig. 7.10, contains the dark green tree, light green grass and the gray separator in the highway(to the right side of frame). For frame 90 the $skcx_4$ only contains the dark green tree as shown in Fig. 7.11. This leads to the different average wavelengt values depicted in Fig. 7.12. When the differences are added up as per the euclidean distance as in Def. 7, this leads to $\delta^2_\Phi(\mathcal{V}_{40}, \mathcal{V}_{90}) = 1$.

Each of these examples depicted in Figs. 5, 6 and 7 illustrate the utility of considering the descriptive similarity of maximal centroidal vortices across the frames. We have seen that the ϕ_{vrt}(vertex based probe function) imposes a more strict notion of similarity than the ϕ_{avg}(region based probe function). Moreover, we saw that there are limits to the flexibility of ϕ_{avg}, since too much change in either the description of regions or structure of the underlying triangulation can result in the frames being marked as dissimilar.

6. Conclusions

In this paper, we have introduced a proximity based framework for the study of videos. We start by developing the notion of maximal centroidal cycles and establishing their relation to the spoke complexes. Further, we have defined the notion of iso-proximal complex and cycle, explaining how they encode the proximity structure of a triangulated space. We establish that spoke complexes and maximal centroidal cycles are iso-proximal.

After having developed the structure to encode the spatial proximity in a video frame, we use the notion of vertex and region based probe functions to track the features along these cycles. This yields a framework that combines the spatial and descriptive proximity to analyze a video frame. We calculate the proposed features on each frame and then find out which frames across the video are descriptively similar. This results in a descriptive frame recurrence diagram. We analyze in great detail how the vertex and region based probes differ in terms of detecting similar frames.

References

Ahmad, M.Z. and J.F. Peters (2017). Proximal čech complexes in approximating digital image object shapes. theory and application. *Theory and Applications of Mathematics & Computer Science* **7**(2), 81–123.

Ahmad, M.Z. and J.F. Peters (2018). Descriptive cellular homology. *arXiv preprint arXiv:1801.01911*.

Alexandroff, P. (1926). Simpliziale approximationen in der allgemeinen topologie. *Mathematische Annalen* **101**(1), 452–456. MR1512546.

Alexandroff, P. (1928). Über den algemeinen dimensionsbegriff und seine beziehungen zur elementaren geometrischen anschauung. *Math. Ann.* **98**, 634.

Alexandroff, P. (1965). *Elementary concepts of topology*. Dover Publications, Inc.. New York. 63 pp., translation of Einfachste Grundbegriffe der Topologie [Springer, Berlin, 1932], translated by Alan E. Farley , Preface by D. Hilbert, MR0149463.

Alexandroff, P. and H. Hopf (1935). *Topologie. Band I*. Springer. Berlin. Zbl 13, 79; reprinted Chelsea Publishing Co., Bronx, N. Y., 1972. iii+637 pp., MR0345087.

Borsuk, K. (1948). On the imbedding of systems of compacta in simplicial complexes. *Fund. Math.* **35**, 217–234. MR0028019.

Borsuk, K. (1975). *Theory of Shape*. Monografie Matematyczne, Tom 59. [Mathematical Monographs, Vol. 59] PWN—Polish Scientific Publishers. MR0418088, Based on K. Borsuk, Theory of shape, Lecture Notes Series, No. 28, Matematisk Institut, Aarhus Universitet, Aarhus, 1971, MR0293602.

Borsuk, K. and J. Dydak (1980). What is the theory of shape?. *Bull. Austral. Math. Soc.* **22**(2), 161–198. MR0598690.

Cooke, G.E. and R.L. Finney (1967). *Homology of cell complexes. Based on lectures by Norman E. Steenrod*. Princeton University Press and University of Tokyo Press. Princeton, N.J., USA; Tokyo, Japan. xv+256 pp., MR0219059.

Edelsbrunner, H. and J.L. Harer (2010). *Computational Topology. An Introduction*. Amer. Math. Soc.. Providence, RI. xii+241 pp. ISBN: 978-0-8218-4925-5, MR2572029.

Munch, E. (2013). Applications of Persistent Homology to Time Varying Systems. PhD thesis. Duke University. Department of Mathematics. supervisor: J. Harer, MR3153181.

Naimpally, S.A. and B.D. Warrack (1970). *Proximity Spaces*. Cambridge Tract in Mathematics No. 59. Cambridge University Press. Cambridge,UK. x+128 pp., ISBN 978-0-521-09183-1, MR2573941.

Peters, J.F. (2013). Near sets: An introduction. *Math. in Comp. Sci.* **7**(1), 3–9. DOI 10.1007/s11786-013-0149-6, MR3043914.

Smirnov, Ju. M. (1964). On proximity spaces. In: *American Math. Soc. Translations, Series 2, vol. 38* (AMS, Ed.). pp. 3–36. Amer. Math. Soc.. Providene, RI.